Preprint of
R. Sevilla and E. Barbieri
NURBS distance fields for extremely curved cracks
Computational Mechanics, 54 (6); 1431-1446, 2014

NURBS distance fields for extremely curved cracks

Ruben Sevilla[1], Ettore Barbieri[2]

[1] *Civil and Computational Engineering Centre (C^{2}EC), College of Engineering, Swansea University, Singleton Park, Swansea, SA2 8PP, Wales, UK.*

[2] *School of Engineering and Materials Science, Queen Mary University of London, Mile End Road, London E1 4NS, UK.*

Abstract

This paper proposes for the first time an intrinsic enrichment for extremely curved cracks in a meshfree framework. The unique property of the proposed method lies in the *exact* geometric representation of cracks using non-uniform rational B-splines (NURBS). A distance function algorithm for NURBS is presented, resulting in a spatial field which is simultaneously discontinuous over the (finite) curved crack and continuous all around the crack tips. Numerical examples show the potential of the proposed approach and illustrate its advantages with respect to other techniques usually employed to model fracture, including standard finite elements with remeshing and the extended finite element method (XFEM). This work represents a further step in an ongoing effort in the community to integrate computer aided design (CAD) with numerical simulations.

Keywords: Cracks, NURBS, Enrichments, Distance fields, Patterns

1. Introduction

Various breath-taking natural landscapes that we observe today are the results of millennial crack propagation at very large scales. Other eye-catching patterns can be observed at much smaller length scales, like glazing in pottery or mud cracks in dried out fields. Less pleasant cracks for cars are those forming on asphalt pavements, known as *crocodile cracking*. Indeed, the patterns observed on the skin of a crocodile's head are due to the

Email addresses: R.Sevilla@swansea.ac.uk (Ruben Sevilla[1]), e.barbieri@qmul.ac.uk (Ettore Barbieri[2])

Preprint of
R. Sevilla and E. Barbieri
NURBS distance fields for extremely curved cracks
Computational Mechanics, 54 (6); 1431-1446, 2014

fragmentation of a thin layer of hard keratin that can be explained with the tools of fracture mechanics [36].

Researchers over the years have tried to replicate experimentally these patterns, or to create new ones artificially. A particularly effective technique is to use solid thin films bonded to elastic substrates. An interesting crack path is the *spiral*, which was probably first reported in [1]. The authors observed experimentally helical paths in thin brittle adhesive layers bonding together Pyrex plates under biaxial tension. The theoretical explanation for this pattern was given many years later by [51], as a competition between propagating along a straight inclined path and the tendency of parallel cracks to reciprocally attract each other. The formation of spiral cracks in fragments of desiccated thin layers of precipitates for different compounds was shown in [26, 32]. The *characteristic length* of these spirals is 1mm, and they form by folding of the layers over a substrate, caused by the shrinking of the layer during the drying process. Whilst helical crack paths are usually observed in skewed cracks under torsional loadings [10], as for example happens when trying to break a piece of chalk, counter-intuitively spiral patterns can be obtained in two dimensional samples without requiring a torsional loading.

Other interesting crack patterns are *wavy* cracks that develop in thin silicate sol-gel films by varying the film thickness, the curing time and the curing temperature, as shown in [40]. Highly ordered wavy cracks have been observed by [50] in silica films on a silicon substrate, where a transition from a sinusoidal pattern to a *crescent sawtooth periodic* structure similar to the patterns presented in [40] has been reported, where the wavelength is of order of 1μm. This behaviour has been explained by a combined effect of in-plane loadings and interface debonding and different applications have recently arisen, including the identification of crack patterns as *signatures* to characterize paintings, see for instance [24]. Other examples of wavy cracks can be found in drying of colloidal dispersions [18], where oscillating crack paths originate in drying films, in tensile loading normal to the average direction of crack growth. Using a *maximum strain energy release rate* criterion instead of a maximum hoop stress criterion, the authors showed that it is possible to predict an oscillatory crack path with the corresponding wavelength. A patterning technique in a Si_3N_4 thin film deposited on a silicon substrate was developed in [30], showing that oscillating crack paths, wide a few nanometres, can be drawn in a controllable manner. Very recently, in [29] the crack resistance of biological systems like teeth and nacre was imitated. Jigsaw-like cracks were engraved on glass with the aim of exploiting their

Preprint of
R. Sevilla and E. Barbieri
NURBS distance fields for extremely curved cracks
Computational Mechanics, 54 (6); 1431-1446, 2014

interlocking behaviour. It was shown that the dissipated energy in *unlocking* these patterns by frictional sliding can significantly enhance the toughness of brittle materials.

A classical problem in the modelling of fracture is the computation of the displacement and stress fields in solids containing cracks. Despite fracture problems of scientific relevance often involve curved cracks, the immense majority of numerical methods developed for modelling fracture discretise the cracks using faceted surfaces or polygonal segments. Other approaches based on high-order methods are able to consider curved finite elements but, even with high-order curved isoparametric elements, the geometric errors have the potential to introduce severe effects on the accuracy of finite element (FE) simulations, see for instance [43].

The relevance of an accurate geometric representation in FE analysis motivated in the late 1990s the incorporation of powerful computer aided design (CAD) techniques into FE computations [12]. More recently, methods able to incorporate the most extended CAD technology, namely non-uniform rational B-splines (NURBS), into the FE analysis stage such as isogeometric methods [23, 13] or the NURBS-enhanced finite element method (NEFEM) [44, 42, 25] have become very popular.

This work proposes for the first time the incorporation of the NURBS description of cracks into a meshfree method for modelling fracture in brittle materials. Among the most prominent methods for fracture, meshfree methods are some of the most mature and established. In solid mechanics, the papers by Belytschko and co-workers [8, 7, 9] on element-free Galerkin (EFG), contemporary with the papers by W. K. Liu and co-workers [28, 27, 11] on reproducing kernel particle method (RKPM), started a stream of a long series of meshfree methods for linear and non-linear solid mechanics developed in the following years. An incomplete list includes the *hp*-clouds [15], the finite point method [34], the free-mesh method [54], the meshless local Petrov-Galerkin (MLPG) [2], the local boundary integral equation (LBIE) [55], the natural element method [47], the meshless finite element method (MFEM) [22] and the cracking particles method [37]. For a complete review of these methods and the history, the interested reader is referred to [17, 33, 3].

An intrinsic enrichment for meshfree methods based on a NURBS distance function is presented. Recently, [6, 4, 5] proposed a *distance function*-based intrinsic enrichment for two and three dimensional problems, able to introduce multiple interacting fracture surfaces tessellated with piecewise segments or non-planar polygons. This paper presents a significant extension

Preprint of
R. Sevilla and E. Barbieri
NURBS distance fields for extremely curved cracks
Computational Mechanics, 54 (6); 1431-1446, 2014

to these methods, allowing cracks to be introduced as NURBS curves. Validation examples, where analytical or reference solutions are available, have been used to demonstrate the applicability and show the accuracy of the proposed methodology. More challenging examples show the potential of the proposed method compared to other approaches such as finite elements with remeshing or extended formulations. Compared to standard FE techniques, the proposed technique does not require meshing geometries containing complex cracks. This is of particular importance when high-order finite elements are combined with remeshing strategies as the generation of curved mesh is particularly complex [52]. Compared to the extended finite element method (XFEM), the proposed approach is able to produce crack branching or crack interaction by adding a single NURBS enrichment and without the need of special enrichments for branching or special care for junctions. Compared to standard meshfree methods, the proposed approach allows the incorporation of the *exact* crack description, understood as the NURBS description, instead of using an approximated geometry representation. It is worth noting that the enrichment process described in this paper can be understood as a modification of the *visibility* condition that has been extensively used in a meshfree framework, see for instance [20, 37, 38, 45, 46]. For a detailed discussion on the advantages of the proposed enrichment with respect to the visibility condition, the reader is referred to [5, 6].

This paper is organized as follows. In Section 2 a model fracture problem is formulated and its numerical solution using the RKPM is briefly summarised. Section 3 presents the fundamentals of NURBS curves, used here for the exact representation of curved cracks. In Section 4 the proposed enrichment, based on the distance function for NURBS curves is presented. Two validation examples are presented in Section 5 in order to demonstrate the applicability of the proposed method for problems where an analytical or reference solution is available. More challenging examples are presented in Section 6, demonstrating the potential of the proposed methodology. The main conclusions of the work are summarised in Section 7. Finally, details of the RKPM approximation and the NURBS data corresponding to the validation examples presented here are described in Appendices Appendix A and Appendix B respectively.

Preprint of
R. Sevilla and E. Barbieri
NURBS distance fields for extremely curved cracks
Computational Mechanics, 54 (6); 1431-1446, 2014

2. Problem formulation

Let us consider an open bounded domain Ω with closed boundary $\Gamma = \partial\Omega$ and containing cracks of various shapes (e.g., v-shaped, branching cracks, cross cracks), as illustrated in Figure 1. The boundary of the domain is partitioned into the Neumann boundary Γ_N, the Dirichlet boundary Γ_D and the internal cracks $\{\Gamma_C^i\}_{i=1}^{N_C}$, where N_C denotes the number of cracks.

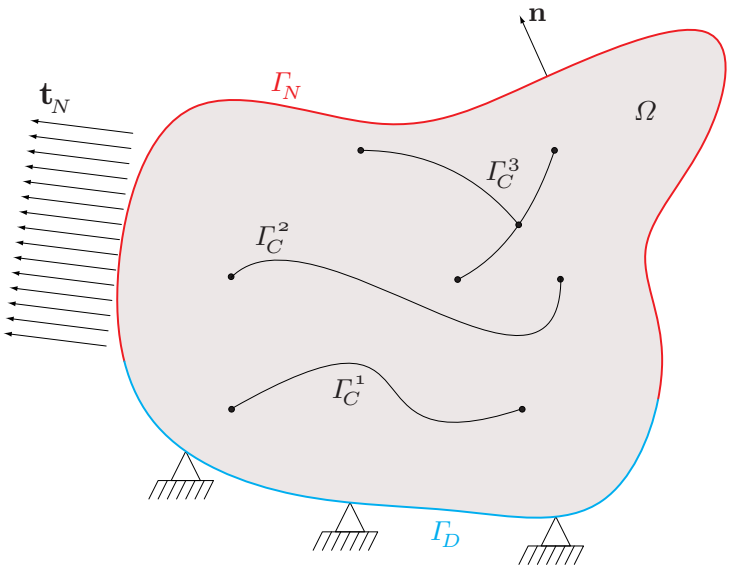

Figure 1: A two dimensional body Ω with three cracks, Γ_C^1, Γ_C^2 and Γ_C^3.

The strong form of the equilibrium equations and the boundary conditions are, in absence of body forces and in the *current configuration*,

$$\nabla \cdot \boldsymbol{\sigma} = \mathbf{0} \qquad \text{in } \Omega \tag{1a}$$

$$\boldsymbol{\sigma} \cdot \mathbf{n} = \mathbf{t}_N \qquad \text{on } \Gamma_N \tag{1b}$$

$$\boldsymbol{\sigma} \cdot \mathbf{n} = \mathbf{0} \qquad \text{on } \bigcup_{i=1}^{N_C} \Gamma_C^i \tag{1c}$$

$$\mathbf{u} = \mathbf{u}_D \qquad \text{on } \Gamma_D \tag{1d}$$

where $\boldsymbol{\sigma}(\mathbf{u})$ is the Cauchy stress tensor, $\mathbf{n}$ is the outward unit normal vector to Γ_N, $\mathbf{t}_N$ is the imposed traction on Γ_N and $\mathbf{u}_D$ is the imposed displacement

Preprint of
R. Sevilla and E. Barbieri
NURBS distance fields for extremely curved cracks
Computational Mechanics, 54 (6); 1431-1446, 2014

on Γ_D. It is worth noting that this work considers cracks in brittle fracture which are tractionless as indicated by the homogeneous Neumann boundary condition (1c). In other situations, such as in cohesive fracture, or for interfaces at dissimilar materials, other boundary conditions are required on the cracks [53].

The weak variational formulation associated to the strong form (1) can be expressed as: find $\mathbf{u} \in [\mathcal{H}_1(\Omega)]^d$ such that

$$\int_\Omega \nabla^s \mathbf{v} : \boldsymbol{\sigma} d\Omega + \beta \int_{\Gamma_D} \mathbf{v} \cdot (\mathbf{u} - \mathbf{u}_D) d\Gamma = \int_{\Gamma_N} \mathbf{v} \cdot \mathbf{t}_N d\Gamma, \qquad \forall \mathbf{v} \in [\mathcal{H}_1(\Omega)]^d \quad (2)$$

where d is the number of spatial dimensions and β is the so-called penalty parameter, a positive scalar constant that must be large enough to accurately impose the Dirichlet boundary condition (1d), see [16] for more details.

Given a set of particles $\{\mathbf{x}_I\}_{I=1}^N$, the solution is approximated as

$$\mathbf{u}(\mathbf{x}) \simeq \mathbf{u}^h(\mathbf{x}) = \sum_{I=1}^{N} \phi_I(\mathbf{x}) \mathbf{U}_I \quad (3)$$

where $\mathbf{U}_I$ is the displacement at particle $\mathbf{x}_I$ and $\phi_I(\mathbf{x})$ is the shape function associated to particle $\mathbf{x}_I$, see an example in Figure 2. Among all the possible alternatives for the approximation, see for instance [21], the reproducing kernel particle method (RKPM) [28] is considered here. The details about the construction of shape functions in the RKPM can be found in the Appendix Appendix A.

Substituting the approximation (3) in the weak form (2) and selecting the space of weighting functions to be equal to the space of approximation functions, results in the non-linear system of equations

$$\mathbf{F}(\mathbf{U}) := \mathbf{F}^i(\mathbf{U}) - \mathbf{F}^e + \mathbf{F}^D(\mathbf{U}) = \mathbf{0} \quad (4)$$

where $\mathbf{U}$ is the vector of nodal values, $\mathbf{F}^i$ is the vector of *internal forces*, given by

$$\mathbf{F}^i(\mathbf{U}) = \int_\Omega \mathbf{B}^T \boldsymbol{\sigma} d\Omega \quad (5)$$

Preprint of
R. Sevilla and E. Barbieri
NURBS distance fields for extremely curved cracks
Computational Mechanics, 54 (6); 1431-1446, 2014

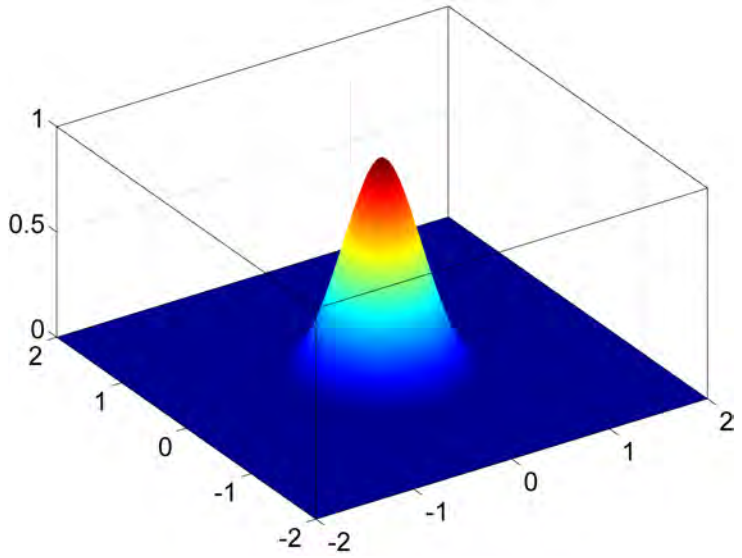

Figure 2: Shape function $\phi_I(\mathbf{x})$ associated to particle $\mathbf{x}_I = (0, 0)$.

$\mathbf{F}^e$ is the vector of *external forces*, given by

$$\mathbf{F}^e = \int_{\Gamma_N} \boldsymbol{\phi}^T \mathbf{t}_N d\Gamma \tag{6}$$

and

$$\mathbf{F}^D(\mathbf{U}) = \beta \left(\int_{\Gamma_D} \boldsymbol{\phi}^T (\mathbf{u} - \mathbf{u}_D) d\Gamma \right) \tag{7}$$

In the above equations, $\boldsymbol{\phi} = (\phi_1, \phi_2, \ldots, \phi_N)$ and $\mathbf{B} = \nabla^s \boldsymbol{\phi}$.

In general, the vector of internal forces, $\mathbf{F}^i$, is non-linear because of the constitutive law (e.g., hyperelasticity or plasticity) and/or due to geometric non-linearities (e.g., large deformations or large strains). In some cases, the vector of external forces, $\mathbf{F}^e$, is also non-linear, for instance when the loads follow the deformed surface, but for the sake of simplicity, this case is not considered in this work.

The system of equations (4) contains several non-linearities even in the case of linear elastic materials, for instance the *self-contact* enforcement at crack surfaces introduces a *contact* non-linearity. To solve this system of non-linear equations, a standard Newton-Raphson iteration is employed, requiring the computation of the Jacobian $\partial \mathbf{F} / \partial \mathbf{U}$. At each Newton-Raphson iteration,

Preprint of
R. Sevilla and E. Barbieri
NURBS distance fields for extremely curved cracks
Computational Mechanics, 54 (6); 1431-1446, 2014

the following linear system of equations is solved

$$\frac{\partial \mathbf{F}(\mathbf{U}_k)}{\partial \mathbf{U}} \Delta \mathbf{U}_k = -\mathbf{F}(\mathbf{U}_k) \tag{8}$$

where the k-th iterative approximation of the solution is denoted by $\mathbf{U}_k$ and $\Delta \mathbf{U}_k = \mathbf{U}_{k+1} - \mathbf{U}_k$. The Jacobian $\partial \mathbf{F}/\partial \mathbf{U}$ depends on the constitutive model of the material and includes also geometric non-linearities, due to non-linear measures of the strain. For instance, in linear elasticity, and using the generalized Hooke's law, it takes the form

$$\left(\frac{\partial \mathbf{F}^i(\mathbf{U})}{\partial \mathbf{U}} \right)_{I,J} = \int_\Omega \mathbf{B}_I^T \mathbf{D} \mathbf{B}_J d\Omega \tag{9}$$

where the *stiffness* tensor, $\mathbf{D}$, and the *infinitesimal strain* tensor, $\boldsymbol{\epsilon}$, expressed with Voigt notation, satisfy $\boldsymbol{\sigma} = \mathbf{D}\boldsymbol{\epsilon}$.

3. Geometric description of cracks using NURBS

This work proposes the use of NURBS to accurately describe the geometry of the cracks $\{\Gamma_C^i\}_{i=1}^{N_C}$ within the domain Ω. This section introduces the fundamentals of NURBS curves. A complete presentation can be found in [35, 39].

A qth-degree NURBS curve is a piecewise rational function defined in parametric form as

$$\boldsymbol{C}(\lambda) = \left(\sum_{i=0}^{N_{cp}} \nu_i \, \boldsymbol{P}_i \, C_i^q(\lambda) \right) \Big/ \left(\sum_{i=0}^{N_{cp}} \nu_i \, C_i^q(\lambda) \right) \qquad \lambda_0 \leq \lambda \leq \lambda_{N_k} \tag{10}$$

where $\{\boldsymbol{P}_i\}$ are the coordinates of the $N_{cp}+1$ *control points* (forming the *control polygon*), $\{\nu_i\}$ are the control weights, and $\{C_i^q(\lambda)\}$ are the normalized B-spline basis functions of degree q, which are defined recursively by

$$C_i^0(\lambda) = \begin{cases} 1 & \text{if } \lambda \in [\lambda_i, \lambda_{i+1}[, \\ 0 & \text{elsewhere,} \end{cases}$$

$$C_i^k(\lambda) = \frac{\lambda - \lambda_i}{\lambda_{i+k} - \lambda_i} C_i^{k-1}(\lambda) + \frac{\lambda_{i+k+1} - \lambda}{\lambda_{i+k+1} - \lambda_{i+1}} C_{i+1}^{k-1}(\lambda)$$

Preprint of
R. Sevilla and E. Barbieri
NURBS distance fields for extremely curved cracks
Computational Mechanics, 54 (6); 1431-1446, 2014

for $k = 1 \dots q$, where λ_i, for $i = 0, \dots, N_k$, are the *knots* or *breakpoints*, which are assumed ordered $0 \leq \lambda_i \leq \lambda_{i+1} \leq 1$. They form the so-called *knot vector*

$$\Lambda = \{\underbrace{\lambda_0, \dots, \lambda_q}_{q+1}, \lambda_{q+1}, \dots, \lambda_{N_k-q-1}, \underbrace{\lambda_{N_k-q}, \dots, \lambda_{N_k}}_{q+1}\} \tag{11}$$

which uniquely describes the B-spline basis functions. The multiplicity of a knot, when it is larger than one, determines the decrease in the number of continuous derivatives. It is assumed that the multiplicity of first and last knot is $q+1$ (i.e., $\lambda_0 = \lambda_1 = \ldots = \lambda_q$ and $\lambda_{N_k-q} = \lambda_{N_k-q+1} = \ldots = \lambda_{N_k}$).

The number of control points, $N_{cp}+1$, and knots, N_k+1, are related to the degree of the parametrisation, q, by the relation $N_k = N_{cp} + q + 1$, see [35] for more details. Figure 3 shows the B-spline basis functions for the knot vector

$$\Lambda = \{0, 0, 0, 0.2, 0.4, 0.6, 0.8, 0.8, 1, 1, 1\} \tag{12}$$

Note that NURBS are piecewise rational functions, whose definition changes

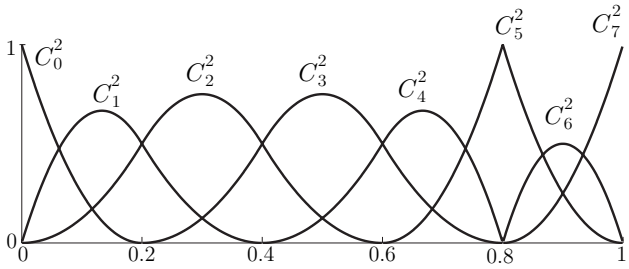

Figure 3: B-spline basis functions for the knot vector (12)

at knots. An example of a NURBS curve is represented in Figure 4 with the

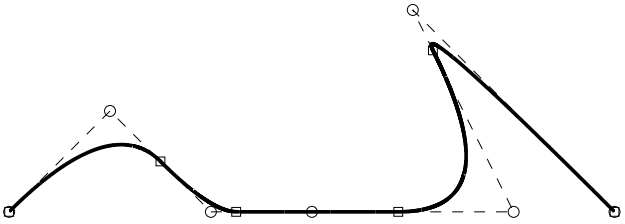

Figure 4: NURBS curve (solid line), control points (denoted by ∘), control polygon (dashed line) and breakpoints (denoted by □)

Preprint of
R. Sevilla and E. Barbieri
NURBS distance fields for extremely curved cracks
Computational Mechanics, 54 (6); 1431-1446, 2014

corresponding control polygon. The image of the breakpoints or knots by the NURBS are depicted in order to stress the discontinuous definition of the parametrisation. In practice CAD manipulators work with *trimmed* NURBS, which are defined as the initial parametrisation restricted to a subspace of the parametric space. Figure 5 shows the NURBS curve of Figure 4 trimmed to the subinterval $[0.05, 0.75]$.

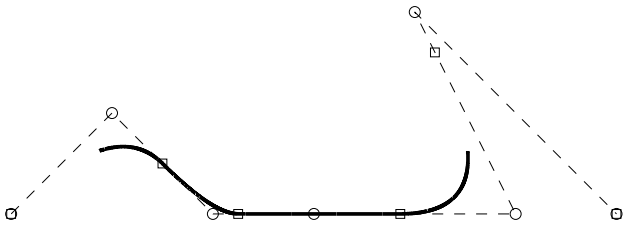

Figure 5: Trimmed NURBS curve with $\lambda \in [0.05, 0.75]$ (solid line), control points (denoted by $\circ$), control polygon (dashed line) and breakpoints (denoted by $\square$)

NURBS curves can also be represented in the so-called *homogeneous* form. For a given set of control points $\{\boldsymbol{P}_i\} = (x_i, y_i, z_i)$ and weights $\{\nu_i\}$, the NURBS curve of Equation (10) can also be represented in the (non-rational) form

$$\boldsymbol{C}(\lambda) = \sum_{i=0}^{N_{cp}} \nu_i \, \boldsymbol{P}_i^{\nu} \, C_i^q(\lambda) \tag{13}$$

where $\boldsymbol{P}_i^{\nu} = (\nu_i x_i, \nu_i y_i, \nu_i z_i, \nu_i)$. This expression is of particular importance for an efficient evaluation of the NURBS curve derivatives.

4. Enrichment based on the NURBS distance function

This section proposes an enrichment function for the particles *near* the cracks. The enrichment is based on the computation of the distance from any point in the domain to a NURBS curve representing a crack.

4.1. NURBS distance function

Let us consider a generic point $\mathbf{x} \in \Omega$ and define the distance function to a NURBS curve parametrised by $\boldsymbol{C}$ as

$$d(\mathbf{x}) := \min_{\lambda \in [\lambda_0, \lambda_{N_k}]} \|\mathbf{x} - \boldsymbol{C}(\lambda)\| \tag{14}$$

Preprint of
R. Sevilla and E. Barbieri
NURBS distance fields for extremely curved cracks
Computational Mechanics, 54 (6); 1431-1446, 2014

The computation of the distance function d involves the solution of a classical problem in the CAD community usually referred as NURBS *point inversion* and *projection*, see for instance [35]. It consists on finding the NURBS parameter $\lambda^{\mathbf{x}}$ such that $d(\mathbf{x}) = \|\mathbf{x} - \boldsymbol{C}(\lambda^{\mathbf{x}})\|$. The point on the curve $\boldsymbol{C}(\lambda^{\mathbf{x}})$ is called the projection of $\mathbf{x}$ on $\boldsymbol{C}$ and it is denoted by $\mathcal{P}(\mathbf{x})$.

A Newton-Raphson iteration strategy is employed in the present work to find the NURBS parameter $\lambda^{\mathbf{x}}$. If the parameter obtained at the k-th iteration is denoted by λ^k, the next approximation is given by

$$\lambda^{k+1} = \lambda^k - \frac{\boldsymbol{C}'(\lambda^k) \cdot \big(\boldsymbol{C}(\lambda^k) - \mathbf{x}\big)}{\boldsymbol{C}''(\lambda^k) \cdot \big(\boldsymbol{C}(\lambda^k) - \mathbf{x}\big) + \|\boldsymbol{C}'(\lambda^k)\|^2} \tag{15}$$

Remark 1. *The iterative scheme of Equation (15) requires a good initial approximation to converge to the solution in few iterations. To this end, the curve is initially sampled and the distance from the point to be projected,* $\mathbf{x}$*, to the sampled points is used to select the initial approximation. The selected number of sample points depends on the complexity and length of the curve that can be initially computed using a composite numerical quadrature [41]. It is important to note that the sampling is done only once and used for projecting all the particles employed by the mesh free approximation. In all the examples presented in this paper, convergence is achieved in less than 6 iterations for the immense majority of the particles, namely for more than 99% of the particles.*

It is worth noting that the distance function $d(\mathbf{x})$ is *clipped* to the initial and final parameters of the curve λ_0 and λ_{N_k}. This is of critical importance when the parameters λ_0 and/or λ_{N_k} are used to trim a NURBS curve, see an example in Figure 4.

For a point $\mathbf{x} \in \Omega$, the intrinsic orthogonal coordinate system given by the tangent and the normal directions to the curve parametrised by $\boldsymbol{C}$ at $\mathcal{P}(\mathbf{x})$ is considered, as illustrated in Figure 6. The position vector of $\mathbf{x}$ in this intrinsic coordinate system can be written as

$$\mathbf{x} - \mathcal{P}(\mathbf{x}) = t\mathbf{t} + n\mathbf{n} \tag{16}$$

where $\mathbf{t}$ and $\mathbf{n}$ denote the tangent and normal directions respectively and

$$t = \mathbf{t} \cdot \big(\mathbf{x} - \mathcal{P}(\mathbf{x})\big), \qquad n = \mathbf{n} \cdot \big(\mathbf{x} - \mathcal{P}(\mathbf{x})\big) \tag{17}$$

Preprint of
R. Sevilla and E. Barbieri
NURBS distance fields for extremely curved cracks
Computational Mechanics, 54 (6); 1431-1446, 2014

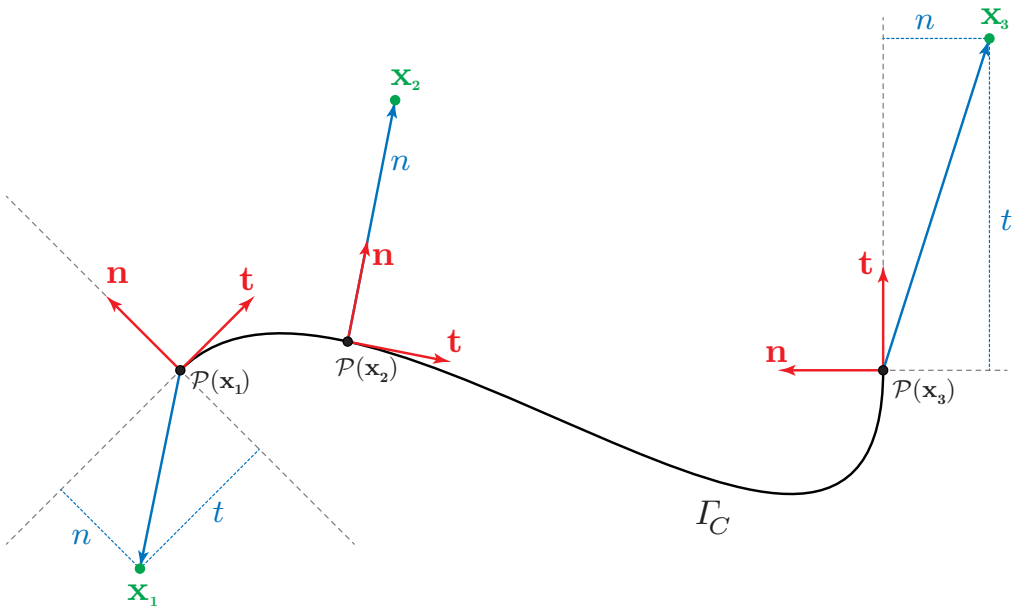

Figure 6: Intrinsic orthogonal coordinate system defined by the tangent and the normal directions to the curve parametrised by $\boldsymbol{C}$ at $\mathcal{P}(\mathbf{x}_i)$ for different points $\mathbf{x}_i$ with $i = 1, 2, 3$.

Preprint of
R. Sevilla and E. Barbieri
NURBS distance fields for extremely curved cracks
Computational Mechanics, 54 (6); 1431-1446, 2014

It is clear that the distance function $d(\mathbf{x})$ can be expressed in terms of the coordinates of $\mathbf{x} - \mathcal{P}(\mathbf{x})$ in the associated intrinsic coordinate system, namely

$$d(\mathbf{x}) = \|\mathbf{x} - \mathcal{P}(\mathbf{x})\| = \sqrt{t^2 + n^2} \tag{18}$$

Figure 7 shows the distance function for a cubic NURBS curve in the domain $\Omega = [-5, 5]^2$. The intrinsic coordinates t and n are represented in Figure 8.

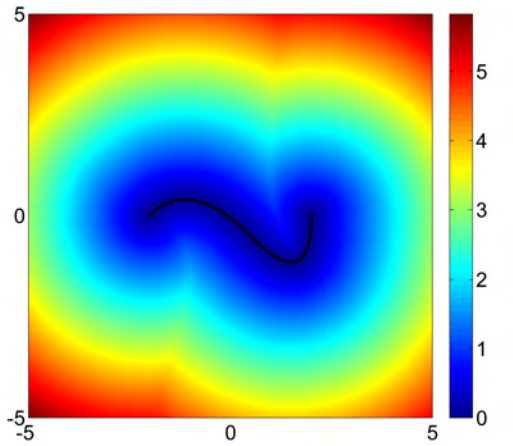

Figure 7: Distance function $d(\mathbf{x})$ in the domain $\Omega = [-5, 5]^2$ with respect to the NURBS curve depicted in black.

Remark 2. *By definition of the projection operator $\mathcal{P}$, when the NURBS parameter of the projected point is not clipped, this is when $\lambda^{\mathbf{x}} \in (\lambda_0, \lambda_{N_k})$, the vector $\mathbf{x} - \mathcal{P}(\mathbf{x})$ lies in the normal direction to the curve and $d(\mathbf{x}) = n$, see an example in Figure 6.*

Remark 3. *The computation of the distance function requires the evaluation of the tangent and normal vectors at a point of a NURBS curve. The classical algorithm presented in [35] is considered here in order to evaluate the tangent to a NURBS curve $\mathbf{t} = (t_1, t_2)$. This algorithm uses the homogeneous representation of the NURBS curve as detalied in Equation (13). The normal is simply $\mathbf{n} = (-t_2, t_1)$, but special attention should be paid when the NURBS curve contains kinks (i.e., points with only $\mathcal{C}^0$ continuity) as the tangent and normal are undefined. The approach proposed here considers in averaging the normal at both sides of the discontinuity. Assuming that a*

Preprint of
R. Sevilla and E. Barbieri
NURBS distance fields for extremely curved cracks
Computational Mechanics, 54 (6); 1431-1446, 2014

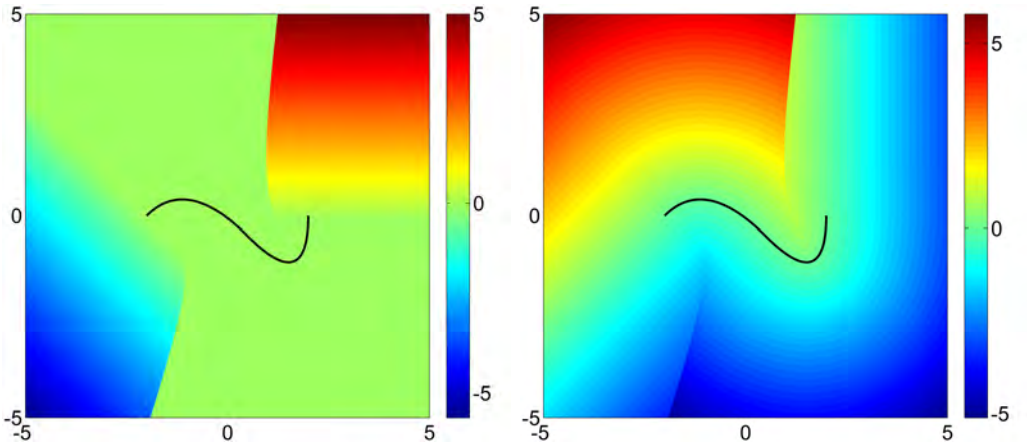

Figure 8: Intrinsic coordinates t (left) and n (right) in the domain $\Omega = [-5, 5]^2$ with respect to the NURBS curve depicted in black.

NURBS curve parametrised by $\boldsymbol{C}$ contains a kink at the parametric coordinate u_g, the following definition of the normal at $\boldsymbol{C}(u_g)$ is proposed

$$\mathbf{n}(u_g) = \frac{1}{2}\left(\lim_{u \to u_g^-} \mathbf{n}(u) + \lim_{u \to u_g^+} \mathbf{n}(u) \right) \tag{19}$$

4.2. The enrichment function

The enrichment function requires the computation of the directional derivatives of the distance function d with respect to the intrinsic coordinates t and n. Using Equation (18), these derivatives are simply given by

$$\frac{\partial d}{\partial t} = \frac{t}{d}, \qquad \frac{\partial d}{\partial n} = \frac{n}{d} \tag{20}$$

and they are illustrated in Figure 9.

In fact, only the derivative in the normal direction is of interest as it is discontinuous across the NURBS curve describing the crack, see Figure 9. The derivative in the normal direction can be seen as a generalisation of the concept of *phase function* introduced in [6, 4, 5] for NURBS curves and it is denoted by

$$\psi := \partial d / \partial n \tag{21}$$

It is worth emphasising that the phase function does not only produce the

Preprint of
R. Sevilla and E. Barbieri
NURBS distance fields for extremely curved cracks
Computational Mechanics, 54 (6); 1431-1446, 2014

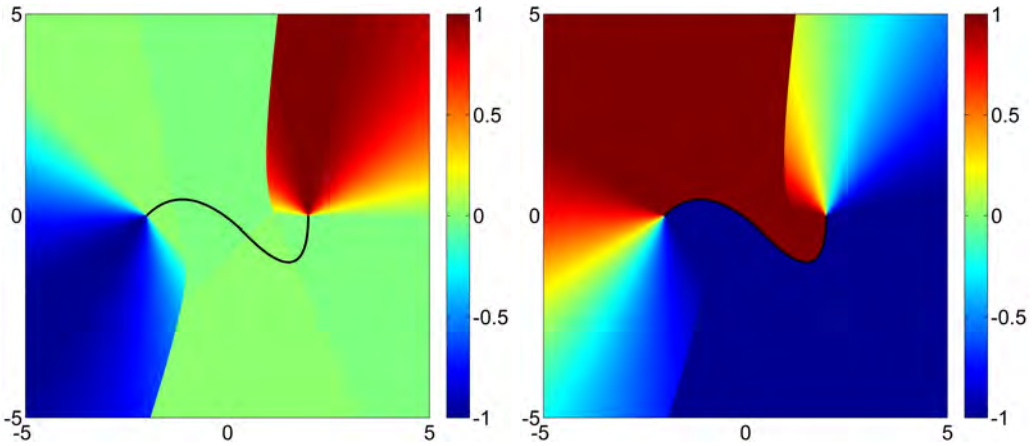

Figure 9: Derivative of the distance function $d(\mathbf{x})$ with respect to the intrinsic coordinates t (left) and n (right) in the domain $\Omega = [-5, 5]^2$ with respect to the NURBS curve depicted in black.

discontinuity required across the crack but it also reflects the angular transition from the upper face and the lower face of the crack, see Figure 9.

The proposed enrichment function is finally defined as

$$h(\mathbf{x}, \mathbf{x}_J) = \left(\frac{1+\psi(\mathbf{x})}{2}\right) H\big(n_{\mathbf{x}_J}\big) + \left(\frac{1-\psi(\mathbf{x})}{2}\right) H\big(-n_{\mathbf{x}_J}\big), \quad \forall J \in \mathcal{S}_{\mathbf{x}}^{\rho} \quad (22)$$

where $n_{\mathbf{x}_J}$ denotes the normal component of $\mathbf{x}_J - \mathcal{P}(\mathbf{x}_J)$ in the intrinsic coordinate system as detailed in Equation (17) and $S_{\mathbf{x}}^{\rho}$ is the index set of particles whose support includes the point $\mathbf{x}$, namely

$$\mathcal{S}_{\mathbf{x}}^{\rho} = \big\{ J \in \{1, 2, \ldots, N\} \quad | \quad \|\mathbf{x} - \mathbf{x}_J\| \leq \rho \big\} \quad (23)$$

and H denotes the Heaviside step function. It is worth noting that

$$H\big(n\big) = \begin{cases} 1 & \text{if} \quad \mathbf{x} \in \Omega^+ \\ 0 & \text{if} \quad \mathbf{x} \in \Omega^- \end{cases}, \qquad H\big(-n\big) = \begin{cases} 0 & \text{if} \quad \mathbf{x} \in \Omega^+ \\ 1 & \text{if} \quad \mathbf{x} \in \Omega^- \end{cases} \quad (24)$$

where the domain Ω has been partitioned in two disjoint subdomains Ω^+ and Ω^- defined as

$$\Omega^+ = \{\mathbf{x} \in \Omega \quad | \quad n \geq 0\}, \qquad \Omega^- = \{\mathbf{x} \in \Omega \quad | \quad n < 0\} \quad (25)$$

Preprint of
R. Sevilla and E. Barbieri
NURBS distance fields for extremely curved cracks
Computational Mechanics, 54 (6); 1431-1446, 2014

as illustrated in Figure 10.

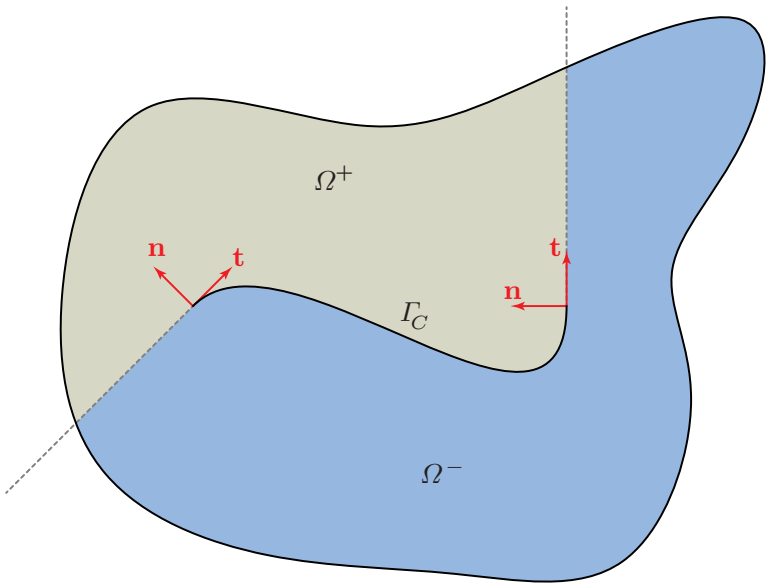

Figure 10: Definition of Ω^+ and Ω^- based on a curved crack Γ_C.

Remark 4. *The definition of the enrichment function* $h(\mathbf{x}, \mathbf{x}_J)$ *in Equation* (22) *remains unchanged if the subdomains* Ω^+ *and* Ω^- *in Equation* (25) *are defined as*

$$\Omega^+ = \{\mathbf{x} \in \Omega \quad | \quad n > 0\}, \qquad \Omega^- = \{\mathbf{x} \in \Omega \quad | \quad n \leq 0\} \tag{26}$$

In both cases, the enrichment function takes a value of 0.5 as $\psi(\mathbf{x}) = 0$ *for particles* $\mathbf{x}$ *such that* $n = 0$.

The enrichment function $h(\mathbf{x}, \mathbf{x}_J)$ of Equation (22) is represented in Figure 11 for a particle in Ω^+ and a particle in Ω^-.

Remark 5. *The phase function* ψ *can be used as an* extrinsic *enrichment for the XFEM. Nonetheless, it requires the scaling and translation introduced in Equation* (22) *in order to create a discontinuity with an* intrinsic *approach.*

For methods based on a Galerkin weak form, it is necessary to compute the derivatives of the shape functions. For those particles that are affected by

Preprint of
R. Sevilla and E. Barbieri
NURBS distance fields for extremely curved cracks
Computational Mechanics, 54 (6); 1431-1446, 2014

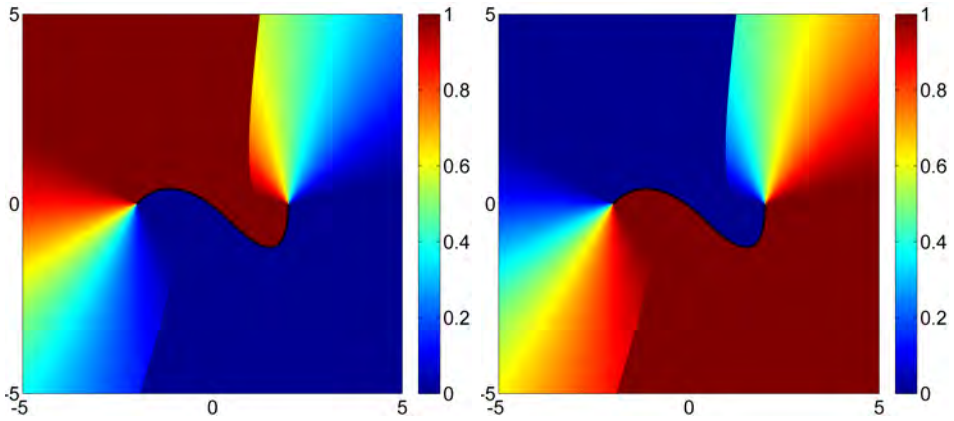

Figure 11: Enrichment function $h(\mathbf{x}, \mathbf{x}_J)$ of Equation (22) for a particle in Ω^+ (left) and a particle in Ω^- (right).

the enrichment function of Equation (22), this involves the derivatives of the enrichment function, which in turn requires the evaluation of the gradient of the phase function in Equation (21), namely

$$\nabla\psi = \frac{1}{d_{\boldsymbol{C}}}\mathbf{n} - \frac{\psi}{d_{\boldsymbol{C}}^2}\big(\mathbf{x} - \mathcal{P}(\mathbf{x})\big) \tag{27}$$

The derivatives of the phase function with respect to x and y coordinates are depicted in Figure 12, illustrating the singular behaviour near the crack tips.

4.3. Selecting the particles to be enriched

Applying the enrichment to all the particles is computationally expensive and unnecessary. The following index set of particles whose support intersects the curve describing the crack is defined

$$\mathcal{S}_{\boldsymbol{C}}^{\rho} = \big\{ J \in \{1, 2, \ldots, N\} \quad | \quad d(\mathbf{x}) \leq \rho \big\} \tag{28}$$

Figure 13 shows a domain Ω with some particles (dots) and their associated support (circles). A continuous line indicates a support of a particle intersecting the crack Γ_C whereas a discontinuous line indicates a support of a particle not intersecting the crack Γ_C. For the particles whose support does not intersect the NURBS curve describing the crack, the standard RKPM approximation is considered and only for the particles whose sup-

Preprint of
R. Sevilla and E. Barbieri
NURBS distance fields for extremely curved cracks
Computational Mechanics, 54 (6); 1431-1446, 2014

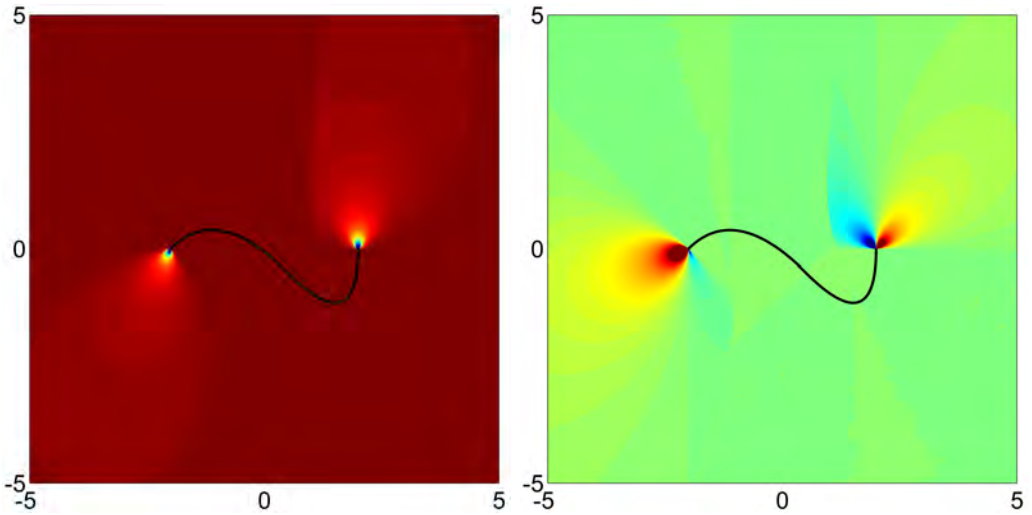

Figure 12: Derivative of the phase function ψ with respect to x (left) and y (right) in the domain $\Omega = [-5, 5]^2$ with respect to the NURBS curve depicted in black.

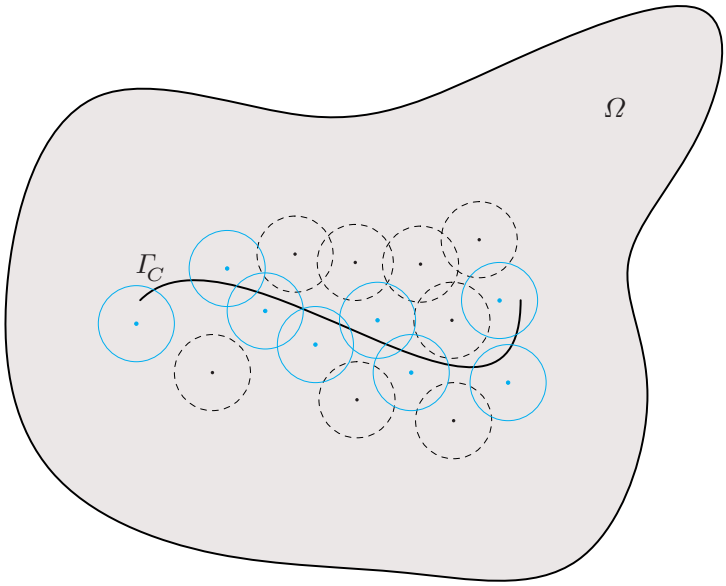

Figure 13: Domain Ω showing particles $\mathbf{x}_I$ such that $I \in \mathcal{S}_C^\rho$ (continuous line denoting their support) and other particles $\mathbf{x}_J$ such that $J \in \mathcal{S}_C^\rho$ (discontinuous line denoting their support)

Preprint of
R. Sevilla and E. Barbieri
NURBS distance fields for extremely curved cracks
Computational Mechanics, 54 (6); 1431-1446, 2014

port intersect the crack the enrichment function proposed in Equation (22) is considered to alter the RKPM shape functions. Therefore, the weighting function appearing in the definition of the RKPM approximation is defined as

$$\omega(\mathbf{x},\mathbf{x}_I) := \begin{cases} \Delta V_I w\left(\frac{\mathbf{x}_I-\mathbf{x}}{\rho}\right) & \text{if} \quad I \notin \mathcal{S}_C^\rho \\ \Delta V_I w\left(\frac{\mathbf{x}_I-\mathbf{x}}{\rho}\right) h(\mathbf{x},\mathbf{x}_I) & \text{if} \quad I \in \mathcal{S}_C^\rho \end{cases} \tag{29}$$

see more details in the Appendix Appendix A.

It is worth mentioning that the objective of selecting a set of particles to be enriched, $\mathcal{S}_C^\rho$, is twofold. First, the local enrichment alleviates the oscillations that typically appear in the stress fields due to the truncation of the approximation kernels. Second, it allows to reduce the computational cost as, usually, the particles to be enriched represent a small percentage of the total number of particles. The additional cost of the enrichment is not only due to the modified definition of the weighting function, but also due to the extra correction required to restore the reproducibility condition of the kernels, see Appendix Appendix A. This is of particular importance when small cracks are considered in relatively large engineering structures.

Figure 14 illustrates the enrichment process for some particles in a domain Ω with a single crack. The two plots show the weighting function defined in Equation (29) for particles in Ω^+ and Ω^- respectively, see Figure 10. Each plot shows the enriched weighting function for some particles whose support intersects the crack and also the standard (non-enriched) weighting function for particles whose support does not intersect the crack.

5. Validation

This section presents the application of the proposed methodology for the computation of the mixed mode Stress Intensity Factors (SIFs). These quantities of engineering interest are extracted from the computed stress fields through the approach described in [19, 49], which accounts for the curvature of the crack path. The procedure is based on computing transforms path-integrals into domain integrals.

Two test cases compromising of an infinite plate with a circular and a parabolic arc crack are considered. For the first example an analytical solution is used to evaluate the accuracy of the proposed methodology. For the second example there is no analytical solution available and a reference

Preprint of
R. Sevilla and E. Barbieri
NURBS distance fields for extremely curved cracks
Computational Mechanics, 54 (6); 1431-1446, 2014

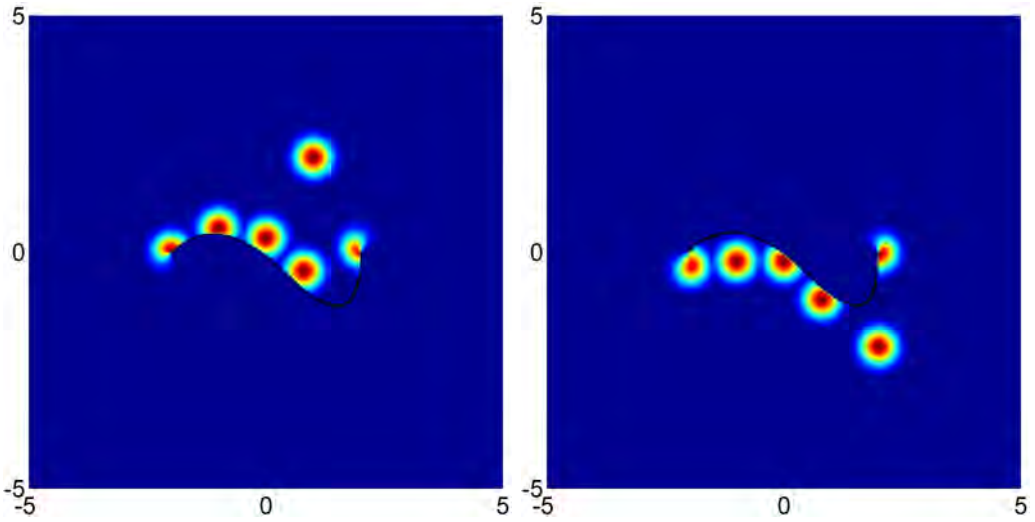

Figure 14: Standard and enriched weighting functions for some particles in Ω^+ (left) and Ω^- (right) in the domain $\Omega = [-5, 5]^2$ with respect to the NURBS curve depicted in black.

solution is used to illustrate consistency with published results obtained with other methods.

5.1. Circular arc crack in an infinite plate

The first example considers an infinite plate with an internal crack in the form of a circular arc subject to a uniaxial tensile loading given by σ^{∞}_{yy}. The geometry of the circular arc is characterised by the chord length $2a$ and the internal angle α as illustrated in Figure 15. The circular arc is exactly represented using the quadratic trimmed NURBS curve detailed in Appendix Appendix B.1. It is important to remark that a circular arc cannot be represented exactly with polynomials and this is, in fact, one of the main advantages of considering NURBS compared to polynomial B-Splines.

For this example, there is an analytical expression for the SIFs [31, 48], namely

$$K_I = \frac{\sigma^{\infty}_{yy}}{2}\sqrt{\pi a}\left[\frac{\left(1-\sin^2\frac{\alpha}{2}\cos^2\frac{\alpha}{2}\right)\cos\frac{\alpha}{2}}{1+\sin^2\frac{\alpha}{2}} + \cos\frac{3\alpha}{2}\right] \tag{30}$$

$$K_I I = \frac{\sigma^{\infty}_{yy}}{2}\sqrt{\pi a}\left[\frac{\left(1-\sin^2\frac{\alpha}{2}\cos^2\frac{\alpha}{2}\right)\sin\frac{\alpha}{2}}{1+\sin^2\frac{\alpha}{2}} + \sin\frac{3\alpha}{2}\right] \tag{31}$$

First, a convergence study is carried out for an plate of length L=1 with

Preprint of
R. Sevilla and E. Barbieri
NURBS distance fields for extremely curved cracks
Computational Mechanics, 54 (6); 1431-1446, 2014

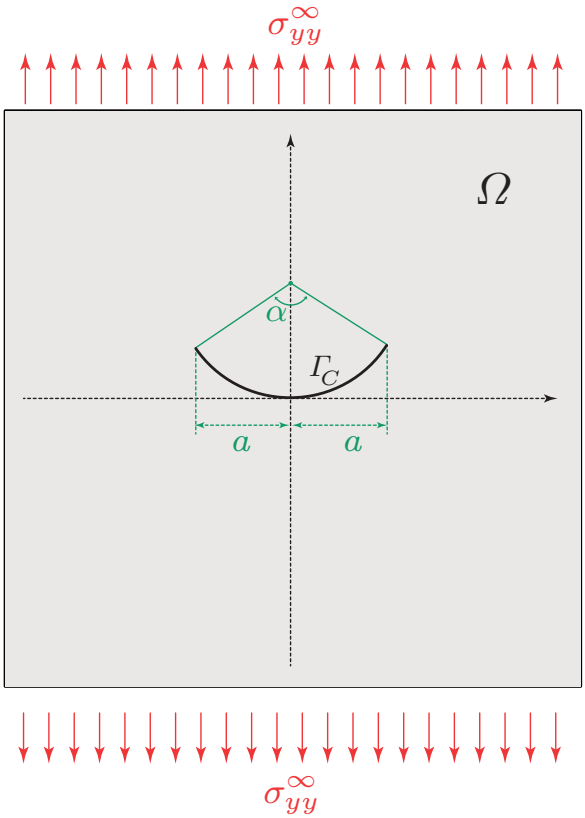

Figure 15: Infinite plate with a circular arc crack under remote uniaxial tensile loading

Preprint of
R. Sevilla and E. Barbieri
NURBS distance fields for extremely curved cracks
Computational Mechanics, 54 (6); 1431-1446, 2014

a circular arc crack characterised by α=$\pi/4$ and a=0.1. The remote uniaxial tensile load is given by σ^{∞}_{yy}=1 Pa. The results in Table 1 show the ratio between the numerical SFIs, K^n_I and K^n_{II}, and the analytical values, K^e_I and K^e_{II}, and the percentage error for different values of the particle spacing h. The coarsest discretisation corresponds to a uniform distribution of 20 $\times$ 20 particles and the finest to a uniform distribution of 150 $\times$ 150 particles, corresponding to a/h=2 and a/h=15 respectively. An excellent accuracy is

Table 1: Convergence of the SIFs for the circular arc crack (Figure 15) with $L = 1$, $a = 0.1$, $\alpha = \pi/4$ and $\sigma^{\infty}_{yy} = 1\ Pa$

a/h	K^n_I/K^e_I	Error [%]	K^n_{II}/K^e_{II}	Error [%]
2	0.4913	50.86	0.4700	53.00
4	0.6481	35.18	0.8566	14.34
10	0.9651	3.48	0.9898	1.02
15	0.9813	1.86	1.0075	0.75

already obtained by using a uniform distribution of 100 $\times$ 100 particles, with an error of approximately 3.5% in K_I and 1% in K_{II}.

Next, the accuracy of the proposed approach is tested for different angles α ranging from 15° up to 60°. In all cases a uniform distribution of 150 $\times$ 150 particles is considered. The results in Table 2 show the ratio between the numerical SFIs, K^n_I and K^n_{II}, and the analytical values, K^e_I and K^e_{II} and the percentage error. The results show, again, an excellent agreement between

Table 2: SIFs for the circular arc crack (Figure 15) for different angles, α, and radius of the arc, R, by using a uniform distribution of 150 $\times$ 150 particles

α	R	K^n_I/K^e_I	Error [%]	K^n_{II}/K^e_{II}	Error [%]
15°	0.3	0.9813	1.87	0.9968	0.29
30°	0.2	1.0032	0.31	1.0199	2.00
60°	0.2	1.0236	2.33	1.0295	2.95

numerical and analytical results, with an error less than 3% in all cases for both K_I and K_{II}.

5.2. Parabolic arc crack in an infinite plate

The second validation example considers an infinite plate with an internal crack in the form of a parabolic arc subject to a remote uniaxial tensile

Preprint of
R. Sevilla and E. Barbieri
NURBS distance fields for extremely curved cracks
Computational Mechanics, 54 (6); 1431-1446, 2014

loading given by σ_{yy}^{∞}. The geometry of the circular arc is characterised by the width of the arc, $2a$, and the focus of the parabola, located at $(0, A)$, as illustrated in Figure 16. The parabolic arc is exactly represented using the

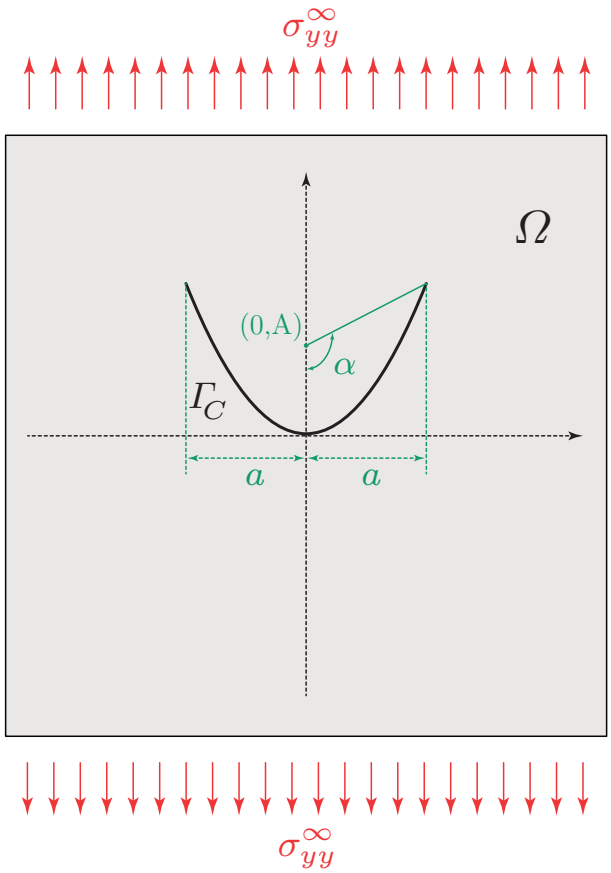

Figure 16: Infinite plate with a parabolic arc crack under remote biaxial load.

quadratic B-Spline curve detailed in Appendix Appendix B.1.

In this case, there is no analytical solution available for the SIFs, but numerically computed curves obtained by a surface integral approach and a discrete piecewise linear representation of the parabola are usually employed to test the accuracy of numerical results. These curves can be found in [31, 48] for a parabola represented with 30 segments. The SIFs can be expressed in a normalized form as

$$K_I = F_I \ \sigma_{yy}^{\infty}\sqrt{\pi a}, \qquad K_{II} = F_{II}\sigma_{yy}^{\infty}\sqrt{\pi a} \tag{32}$$

Preprint of
R. Sevilla and E. Barbieri
NURBS distance fields for extremely curved cracks
Computational Mechanics, 54 (6); 1431-1446, 2014

where F_I and F_{II} are corrective factors of an equivalent central straight crack of length equal to the half-width of the parabolic arc, a. The numerical values of the corrective factors computed with the proposed approach are detailed in Table 3 for a parabolic arc with a=0.05 in a plate of length L=1 by using a uniform distribution of 150 × 150 particles.

Table 3: Corrective factors for the parabolic arc crack (Figure 16) for different angles α, a=0.05 and L=1, by using a uniform distribution of 150 × 150 particles.

α	F_I^n	F_{II}^n
0°	1.0028	0.0016
10°	0.9952	0.0954
20°	0.9762	0.1753
30°	0.9406	0.2623
40°	0.8933	0.3414
50°	0.8369	0.4060
60°	0.7697	0.4639
70°	0.6962	0.5125
80°	0.6092	0.5602
90°	0.5325	0.5818

It is worth noting that the computed values for α=0° correspond to the central straight crack test and, in this case, the exact value of the corrective factors is known to be F_I^e=1 and F_{II}^e=0. Again this results in an error of 2.15% for F_I^n and 0.89% for F_{II}^n, this is a similar accuracy compared to the results of the previous validation example.

The numerical results are also represented in Figure 17 and compared with the results published in [31] as a reference. The results are in excellent agreement and only small discrepancies are observed for the first corrective factor F_I when the angle is $\alpha \geq 70°$. It is worth emphasising that this discrepancy is expected as we provide the solution using the exact description of the parabolic arc whereas the methodology in [31] employs a polygonal approximation of the crack.

6. Numerical examples

This section presents two more challenging examples to illustrate the potential of the proposed technique by using NURBS for describing the geometry of complicated cracks.

Preprint of
R. Sevilla and E. Barbieri
NURBS distance fields for extremely curved cracks
Computational Mechanics, 54 (6); 1431-1446, 2014

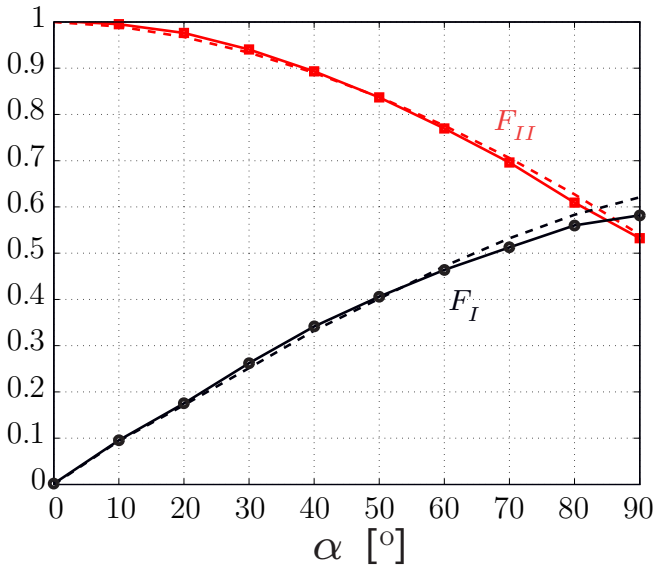

Figure 17: Corrective factors for the parabolic arc obtained with the proposed methodology (continuous line) and reference results extracted from [31] (discontinuous line)

6.1. Spiral cracks

In [51], the authors predicted, theoretically, the emergence of spiral cracks for films bonded to an elastic substrate under a biaxial tensile state. For such systems, biaxial in-plane tensile stresses develop, for example, when there is a mismatch between the two thermal expansion coefficients. Spiral cracks were produced experimentally by [26, 32]. Despite being an intrinsically three-dimensional phenomenon, cracks develop by channelling with an advancing front that becomes straight and orthogonal to the substrate at a steady state, rendering the problem essentially two-dimensional. In [51] it was stated that when the crack length is only slightly greater than the thickness of several films, it can be considered close to steady state.

The approach proposed in this paper allows to reproduce these complex patterns without the need to discretise the cracks in line segments and without the time consuming need to generate a complicated mesh. In addition, and contrary to other approaches, a single enrichment is enough to reproduce the complex physics of these problems. The spiral crack considered here is exactly represented using a cubic NURBS with 300 control points.

Figure 18 shows the intrinsic coordinate n and the phase function ψ introduced in Equations (17) and (21) respectively, for a spiral crack obtained

Preprint of
R. Sevilla and E. Barbieri
NURBS distance fields for extremely curved cracks
Computational Mechanics, 54 (6); 1431-1446, 2014

by the experimental work of [40]. This crack corresponds to a *single arm spiral* of 1mm created in a controlled and reproducible manner in thin silicate sol-gel films by varying the film deposition parameters.

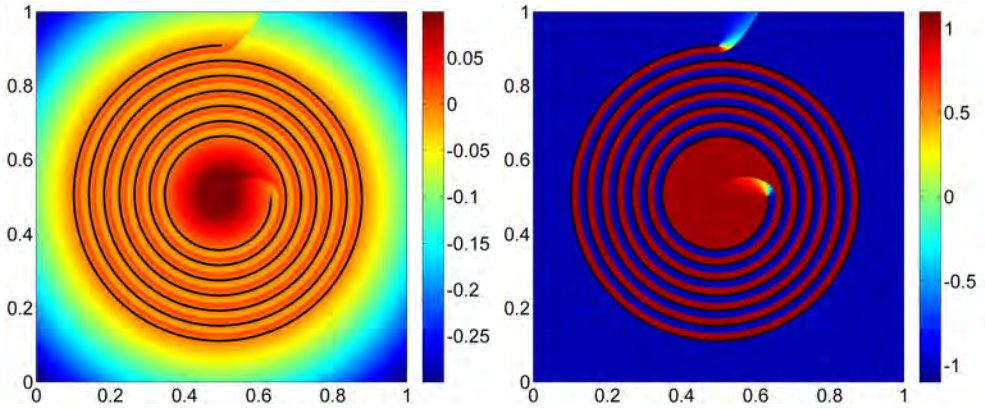

Figure 18: Intrinsic coordinate n (left) and phase function (right) for a domain with a spiral crack

To show the potential and the effectiveness of the proposed enrichment, two different loading conditions are studied.

The first case considers a simple horizontal translation to the specimen as represented in Figure 19. Due to the existing spiral crack, the displacement field, also represented in Figure 19, clearly shows the spiral discontinuity created by the enrichment. The red colour depicts the imposed translation

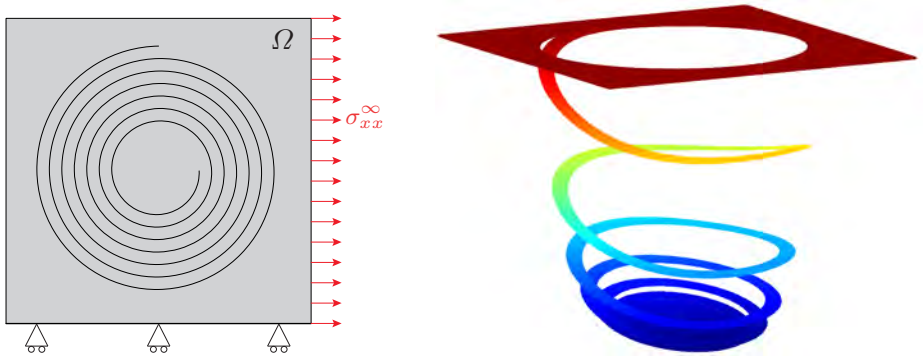

Figure 19: Domain Ω with a spiral crack. Loading condition (left) and magnified displacement (right)

and the blue colour means a decreased displacement. The magnified stress

Preprint of
R. Sevilla and E. Barbieri
NURBS distance fields for extremely curved cracks
Computational Mechanics, 54 (6); 1431-1446, 2014

plot represented in Figure 20 shows the unfolding of the parts of the specimen cut by the spiral: the outer edges of the square are the most displaced, while the most internal spire is the least displaced. All the intermediate values of the displacements (from the innermost spire to the edges of the square sample) cause the *characteristic* swirling of the sample in Figure 20.

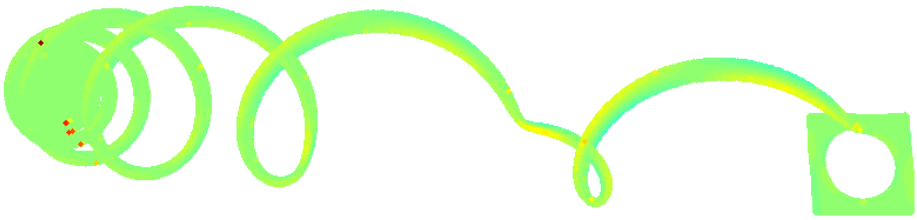

Figure 20: Magnified displacement and σ_{xx}^{∞} stress for the domain with a spiral crack and the loading condition of Figure 19.

The second case considers a biaxial loading applied to the specimen. The displacement field and the magnified stresses are represented in Figure 21, showing that the outermost spire effectively creates a *hole-like* discontinuity in the domain, thus disconnecting the internal spires. This means that the

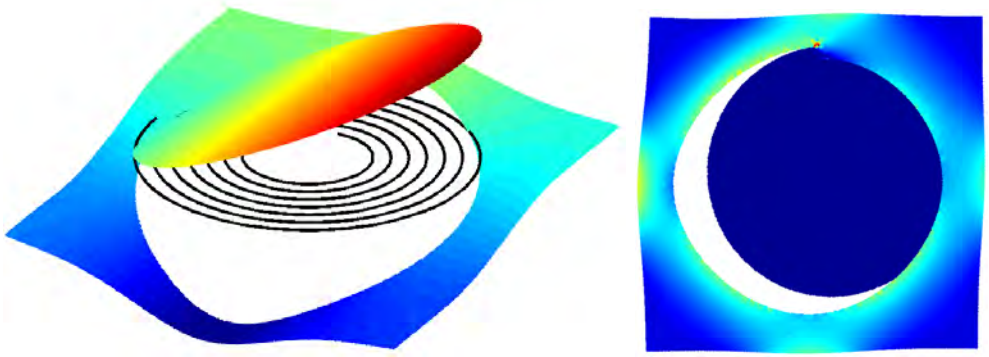

Figure 21: Magnified displacement (left) and magnified deformation with Von misses stress (right) for the domain with a spiral crack and a biaxial loading.

internal spires are unloaded, and that the stresses concentrate only at the boundary of the outermost spire.

Preprint of
R. Sevilla and E. Barbieri
NURBS distance fields for extremely curved cracks
Computational Mechanics, 54 (6); 1431-1446, 2014

6.2. Curved wavy cracks

The last example considered here is based on a curved wavy crack presented in [40]. This example not only shows the potential and effectiveness of the proposed enrichment, but also demonstrates the capability to deal with cracks containing kinks (i.e., points with only $\mathcal{C}^0$ continuity), in this case the kinks developed in sawtooth cracks, and the possibility to consider intersecting cracks without any special treatment. Each curved crack is represented using a cubic NURBS curve with 31 control points and containing two kinks. The domain Ω containing three curved wavy cracks joining at one point is represented in Figure 22, illustrating the applied loads.

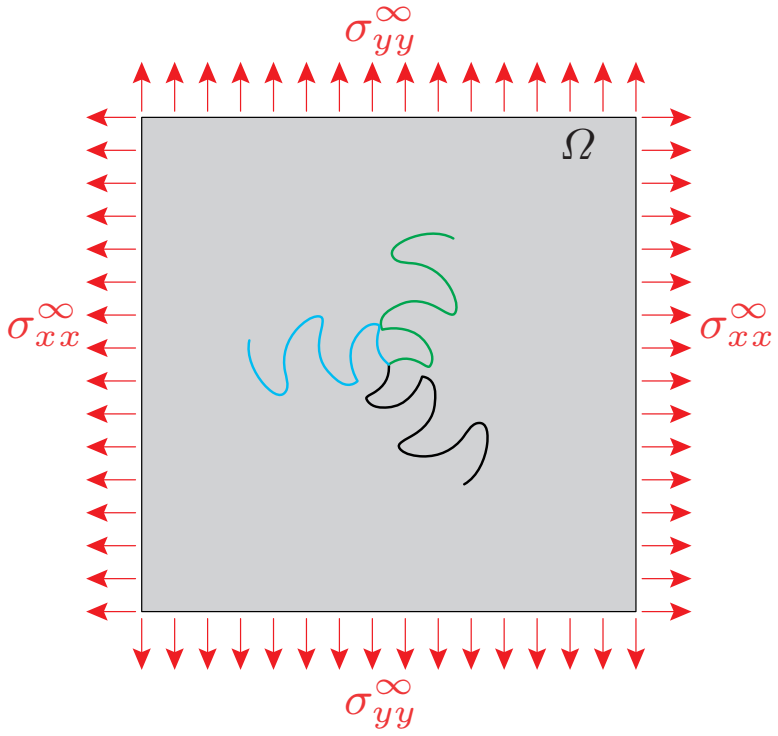

Figure 22: Domain Ω with three wavy cracks joining at a point.

Figure 23 shows the horizontal and vertical displacement obtained with the proposed strategy. It can be observed that the enrichment enforces discontinuities in the displacements over the sawtooth patterns, with no special treatment of the junction between the cracks as it is required with XFEM, see for instance [14]. It is also worth mentioning the ability to handle kinks in

Preprint of
R. Sevilla and E. Barbieri
NURBS distance fields for extremely curved cracks
Computational Mechanics, 54 (6); 1431-1446, 2014

the cracks by computing the normal at the kink using the strategy proposed in Section 4.1. The only contact point between the cracks is the central point

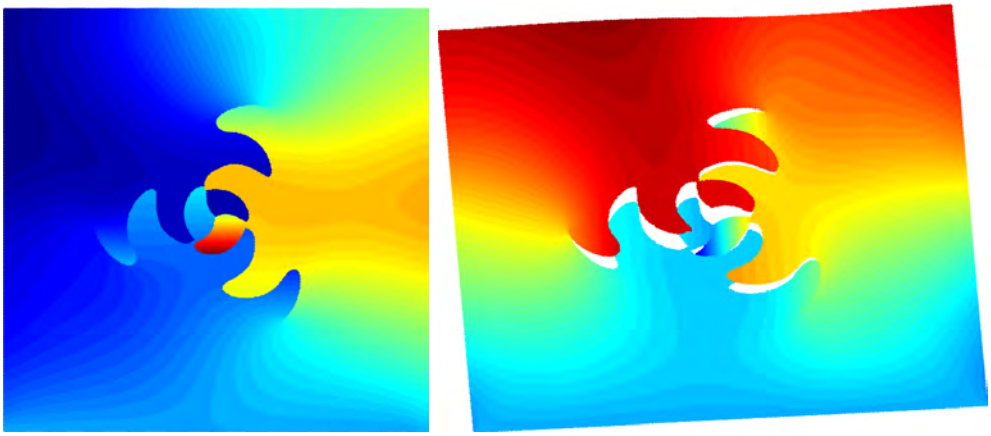

Figure 23: Horizontal (left) and vertical (right) displacement field for the domain with three wavy cracks.

where the three cracks meet. This means that, despite the distance between the two cracks is very small in some regions, there is no separation of the central component of the specimen. This can be better observed in the right plot of Figure 23, where the vertical displacement is displayed.

7. Conclusions

This paper presents, for the first time, an intrinsic enrichment for mesh-free methods based on a NURBS distance function. This represents a significant improvement with respect to previous works in fracture modelling because the uncertainty due to a poor geometric representation of the crack is completely removed. First, the NURBS representation of cracks allows to exactly represent conics and second, it avoids the necessity to discretise complex cracks using polygonal lines or high-order polynomials, reducing the burden of the pre-processing stage and introducing the crack description *faithfully*.

Due to the properties of NURBS curves, it is possible to obtain a low-cost book-keeping of complicated fracture patterns, including complex curved cracks that intersect and/or contain kinks. Compared to other enrichment approaches such as XFEM, the proposed approach is able to produce crack

Preprint of
R. Sevilla and E. Barbieri
NURBS distance fields for extremely curved cracks
Computational Mechanics, 54 (6); 1431-1446, 2014

branching or crack interaction by adding a single NURBS enrichment and without the need of special enrichments for branching or special care for junctions.

Two validation examples, where analytical or reference solutions are available, have been used to demonstrate the applicability and show the accuracy of the proposed methodology. More challenging examples show the superiority of the proposed method compared to other approaches such as finite elements with remeshing or extended formulations. We showed, for example, that the proposed enrichment can simulate highly curved cracks, like spirals or sawtooth, commonly observed in nature on in controlled experiments on thin solid films.

The incorporation of the exact boundary representation obviously introduces an extra cost in terms of the computation of the intrinsic coordinate system. Simple strategies for the computation of the normal and tangent at projected points have been employed in order to show the applicability of the proposed techniques to challenging problems. Further research will include the study of more advanced algorithms proposed by the CAD community in order to reduce the computational cost.

Appendix A. The RKPM approximation

This work considers the reproducing kernel particle method (RKPM) for the functional approximation, see [28]. This method can also be viewed as the result of applying a numerical quadrature to the continuous moving least squares approximation that is usually employed in other meshfree methods such as the element-free Galerkin method, see [21, 8] for more details.

The RKPM shape function associated to a particle $\mathbf{x}_I \in \Omega$ is given by

$$\phi_I(\mathbf{x}) = \omega(\mathbf{x}_I, \mathbf{x})\mathbf{P}^T(\mathbf{x})\mathbf{M}^{-1}(\mathbf{x})\mathbf{P}(\mathbf{x}_I) \tag{A.1}$$

where the weighting function is defined as

$$\omega(\mathbf{x}_I, \mathbf{x}) = \Delta V_I w\Big(\frac{\mathbf{x}_I - \mathbf{x}}{\rho}\Big) \tag{A.2}$$

with $(\Delta V_I, \mathbf{x}_I)$ denoting the quadrature weights and points (particles), $\mathbf{P}(\mathbf{x})$ denotes a complete basis of the subspace of polynomials of degree k, $\mathbf{P}(\mathbf{x}) =$

Preprint of
R. Sevilla and E. Barbieri
NURBS distance fields for extremely curved cracks
Computational Mechanics, 54 (6); 1431-1446, 2014

$\{p_0(\mathbf{x}), p_1(\mathbf{x}), \ldots, p_k(\mathbf{x})\}$, and $\mathbf{M}$ is the so-called *moment matrix*

$$\mathbf{M}(\mathbf{x}) = \sum_{I \in \mathcal{S}_{\mathbf{x}}^{\rho}} \omega(\mathbf{x}_I, \mathbf{x}) \mathbf{P}(\mathbf{x}_I) \mathbf{P}^T(\mathbf{x}_I) \tag{A.3}$$

where the index set $\mathcal{S}_{\mathbf{x}}^{\rho}$ is defined in Equation (23).

The moment matrix $\mathbf{M}$ can also be viewed as a Gram matrix defined with a discrete scalar product

$$\langle u, v \rangle_{\mathbf{x}} = \sum_{I \in \mathcal{S}_{\mathbf{x}}^{\rho}} \omega(\mathbf{x}_I, \mathbf{x}) u(\mathbf{x}_I) v(\mathbf{x}_I) \tag{A.4}$$

and, from a numerical point of view, it is convenient to work with a centred and scaled version to enhance the condition number of the system of normal equations. This correction implies that the following definition of $\mathbf{M}$ is adopted here

$$\mathbf{M}(\mathbf{x}) = \sum_{I \in \mathcal{S}_{\mathbf{x}}^{\rho}} \omega(\mathbf{x}_I, \mathbf{x}) \mathbf{P}\Big(\frac{\mathbf{x}_I - \mathbf{x}}{\rho}\Big) \mathbf{P}^T\Big(\frac{\mathbf{x}_I - \mathbf{x}}{\rho}\Big) \tag{A.5}$$

where ρ denotes the average of all the compact support radii.

The continuity properties of the RKPM shape functions are clearly linked to the continuity properties of the function w in Equation (A.2), see [17], which is usually referred as the *kernel* of the approximation. This work considers the so-called *2k-th order spline*, which is the C^{k-1} function given by

$$w(\xi) = \begin{cases} (1 - \xi^2)^k & 0 \leq \xi \leq 1 \\ 0 & \xi > 1 \end{cases} \tag{A.6}$$

Appendix B. Control data for NURBS objects

This section contains the NURBS description of the two cracks used in Section 5.

Appendix B.1. Circular arc

There are many options to define a NURBS describing a circle. A commonly used options is to define a quadratic NURBS with four rational seg-

Preprint of
R. Sevilla and E. Barbieri
NURBS distance fields for extremely curved cracks
Computational Mechanics, 54 (6); 1431-1446, 2014

ments. The knot vector is

$$\Lambda = \{0, 0, 0, 0.25, 0.5, 0.75, 1, 1, 1\} \tag{B.1}$$

and the control points and weights are detailed in Table B.4 for a circle centred at the origin and with radius R.

i	$\mathbf{P}_i$	ν_i
1	$(-R,\ 0)$	1
2	$(-R,\ -R)$	$\sqrt{2}/2$
3	$(0,\ -R)$	1
4	$(R,\ -R)$	$\sqrt{2}/2$
5	$(R,\ 0)$	1
6	$(R,\ R)$	$\sqrt{2}/2$
7	$(0,\ R)$	1
8	$(-R,\ R)$	$\sqrt{2}/2$
9	$(-R,\ 0)$	1

Table B.4: Control points and weights for a circle of radius R.

In order to define the circular arc depicted in Figure 15, the radius of the circle is taken as $\mathrm{R} = a/\sin(\alpha)$ and the NURBS curve describing a circle is trimmed to the subinterval $[(1-\alpha)/360, 0.5-(1-\alpha)/360]$ where the angle α is given in degrees.

Appendix B.2. Parabolic arc

A parabolic arc can be described using a quadratic B-Spline with just three control points. The knot vector is simply

$$\Lambda = \{0, 0, 0, 1, 1, 1\} \tag{B.2}$$

and the control points for the parabolic arc depicted in Figure 16 are detailed in Table B.5, where $y_a = a^2/(4A)$. The coordinates of the focus of the parabola are $(0, A)$, where $A = a/(2\tan\alpha)$.

Preprint of
R. Sevilla and E. Barbieri
NURBS distance fields for extremely curved cracks
Computational Mechanics, 54 (6); 1431-1446, 2014

i	$\mathbf{P}_i$
1	$(\text{-}a,\ y_a)$
2	$(0,\ -y_a)$
3	$(\ a,\ y_a)$

Table B.5: Control points for a parabolic arc.

References

[1] Argon A (1959) Surface cracks on glass. Proceedings of the Royal Society of London Series A Mathematical and Physical Sciences 250(1263):472–481

[2] Atluri S, Zhu T (1998) A new meshless local Petrov-Galerkin (MLPG) approach in computational mechanics. Computational mechanics 22(2):117–127

[3] Barbieri E, Meo M (2012) A fast object-oriented Matlab implementation of the Reproducing Kernel Particle Method. Computational Mechanics 49(5):581–602

[4] Barbieri E, Petrinic N (2013) Multiple crack growth and coalescence in meshfree methods with a distance function-based enriched kernel. In: Key Engineering Materials - Advances in Crack Growth Modeling, TransTech Publications, p 170

[5] Barbieri E, Petrinic N (2014) Three-dimensional crack propagation with distance-based discontinuous kernels in meshfree methods. Computational Mechanics 53(2):325–342

[6] Barbieri E, Petrinic N, Meo M, Tagarielli V (2012) A new weight-function enrichment in meshless methods for multiple cracks in linear elasticity. International Journal for Numerical Methods in Engineering 90(2):177–195

[7] Belytschko T, Gu L, Lu Y (1994) Fracture and crack growth by element-free Galerkin methods. Modelling Simul Mater Sci Eng 2:519–534

[8] Belytschko T, Lu Y, Gu L (1994) Element-free Galerkin methods. International Journal for Numerical Methods in Engineering 37(2):229–256

Preprint of
R. Sevilla and E. Barbieri
NURBS distance fields for extremely curved cracks
Computational Mechanics, 54 (6); 1431-1446, 2014

[9] Belytschko T, Lu Y, Gu L (1995) Crack propagation by element-free Galerkin methods. Engineering Fracture Mechanics 51(2):295–315

[10] Brokenshire DR (1996) A study of torsion fracture tests. PhD thesis, Cardiff University

[11] Chen JS, Pan C, Wu CT, Liu WK (1996) Reproducing kernel particle methods for large deformation analysis of non-linear structures. Computer Methods in Applied Mechanics and Engineering 139(1):195–227

[12] Cirak F, Ortiz M, Schröder P (2000) Subdivision surfaces: a new paradigm for thin-shell finite-element analysis. International Journal for Numerical Methods in Engineering 47(12):2039–2072

[13] Cottrell JA, Hughes TJ, Bazilevs Y (2009) Isogeometric analysis: toward integration of CAD and FEA. John Wiley & Sons

[14] Daux C, Moes N, Dolbow J, Sukumar N, Belytschko T (2000) Arbitrary branched and intersecting cracks with the extended finite element method. International Journal for Numerical Methods in Engineering 48(12):1741–1760

[15] Duarte CA, Oden JT (1996) Hp clouds-an hp meshless method. Numerical methods for partial differential equations 12(6):673–706

[16] Fernández-Méndez S, Huerta A (2004) Imposing essential boundary conditions in mesh-free methods. Computer Methods in Applied Mechanics and Engineering 193(12-14):1257–1275

[17] Fries T, Matthies H (2003) Classification and overview of meshfree methods. Brunswick, Institute of Scientific Computing, Technical University Braunschweig, Germany Informatikbericht Nr 3

[18] Goehring L, Clegg WJ, Routh AF (2011) Wavy cracks in drying colloidal films. Soft Matter 7(18):7984–7987

[19] Gosz M, Moran B (2002) An interaction energy integral method for computation of mixed-mode stress intensity factors along non-planar crack fronts in three dimensions. Engineering Fracture Mechanics 69(3):299–319

[20] Griebel M, Schweitzer MA (eds) (2008) Meshfree Methods for Partial Differential Equations IV, Lecture Notes in Computational Science and Engineering,, vol 65. Springer

[21] Huerta A, Belytschko T, Fernández-Méndez S, Rabczuk T (2004) Encyclopedia of Computational Mechanics, vol 1. Fundamentals, Wiley, chap Meshfree Methods, pp 279–309

[22] Idelsohn SR, Oñate E, Calvo N, Del Pin F (2003) The meshless finite element method. International Journal for Numerical Methods in Engineering 58(6):893–912

[23] Inoue K, Kikuchi Y, Masuyama T (2005) A NURBS finite element method for product shape design. J Engrg Design 16(2):157–174

[24] Lazarus V, Pauchard L (2011) From craquelures to spiral crack patterns: influence of layer thickness on the crack patterns induced by desiccation. Soft Matter 7(6):2552–2559

[25] Legrain G (2013) A NURBS-enhanced extended finite element approach for unfitted CAD analysis. Computational Mechanics 52(4):913–929

[26] Leung KT, Jozsa L, Ravasz M, Neda Z (2001) Pattern formation: Spiral cracks without twisting. Nature 410(6825):166–166

[27] Liu WK, Jun S, Li S, Adee J, Belytschko T (1995) Reproducing kernel particle methods for structural dynamics. International Journal for Numerical Methods in Engineering 38(10):1655–1679

[28] Liu WK, Jun S, Zhang YI (1995) Reproducing kernel particle methods. International Journal for Numerical Methods in Fluids 20(8-9):1081–1106

[29] Mirkhalaf M, Dastjerdi AK, Barthelat F (2014) Overcoming the brittleness of glass through bio-inspiration and micro-architecture. Nature communications 5

[30] Nam KH, Park IH, Ko SH (2012) Patterning by controlled cracking. Nature 485(7397):221–224

Preprint of
R. Sevilla and E. Barbieri
NURBS distance fields for extremely curved cracks
Computational Mechanics, 54 (6); 1431-1446, 2014

[31] Narendran V, Cleary MP (1984) Elastostatic interaction of multiple arbitrarily shaped cracks in plane inhomogeneous regions. Engineering Fracture Mechanics 19

[32] Neda Z, Jozsa L, Ravasz M, et al (2002) Spiral cracks in drying precipitates. Physical review letters 88(9):095,502

[33] Nguyen V, Rabczuk T, Bordas S, Duflot M (2008) Meshless methods: A review and computer implementation aspects. Mathematics and Computers in Simulation

[34] Oñate E, Idelsohn S, Zienkiewicz O, Taylor R (1996) A finite point method in computational mechanics. applications to convective transport and fluid flow. International Journal for Numerical Methods in Engineering 39(22):3839–3866

[35] Piegl L, Tiller W (1995) The NURBS Book. Springer-Verlag, London

[36] Qin Z, Pugno N, Buehler M (2014) Mechanics of fragmentation of crocodile skin and other thin films. Scientific Reports 4:4966

[37] Rabczuk T, Belytschko T (2004) Cracking particles: a simplified meshfree method for arbitrary evolving cracks. International Journal for Numerical Methods in Engineering 61(13):2316–2343

[38] Rabczuk T, Zi G, Bordas S, Nguyen-Xuan H (2010) A simple and robust three-dimensional cracking-particle method without enrichment. Computer Methods in Applied Mechanics and Engineering 199(37):2437–2455

[39] Rogers DF (2001) An introduction to NURBS with historical perspective. Academic Press, Inc., San Diego, CA

[40] Sendova M, Willis K (2003) Spiral and curved periodic crack patterns in sol-gel films. Applied Physics A 76(6):957–959

[41] Sevilla R, Fernández-Méndez S (2011) Numerical integration over 2D NURBS shaped domains with applications to NURBS-enhanced FEM. Finite Elements in Analysis and Design 47(10):1209–1220

Preprint of
R. Sevilla and E. Barbieri
NURBS distance fields for extremely curved cracks
Computational Mechanics, 54 (6); 1431-1446, 2014

[42] Sevilla R, Fernández-Méndez S, Huerta A (2011) 3D-NURBS-enhanced finite element method (NEFEM). International Journal for Numerical Methods in Engineering 88(2):103–125

[43] Sevilla R, Fernández-Méndez S, Huerta A (2011) Comparison of high-order curved finite elements. International Journal for Numerical Methods in Engineering 87(8):719–734

[44] Sevilla R, Fernández-Méndez S, Huerta A (2011) NURBS-enhanced finite element method (NEFEM): A seamless bridge between CAD and FEM. Archives of Computational Methods in Engineering 18(4):441–484

[45] Simkins D (2012) Multi-scale structural mechanics for advanced aircraft design. Journal of Nonlinear Systems and Applications 3(1):41–45

[46] Simkins D, Li S (2006) Meshfree simulations of thermo-mechanical ductile fracture. Computational Mechanics 38(3):235–249

[47] Sukumar N (1998) The natural element method in solid mechanics. PhD thesis, Northwestern University

[48] Tada H, Paris P, Irwin G (2000) The Stress Analysis of Cracks Handbook. ASME, New York

[49] Walters MC, Paulino GH, Dodds RH (2005) Interaction integral procedures for 3-d curved cracks including surface tractions. Engineering Fracture Mechanics 72(11):1635–1663

[50] Wan N, Xu J, Lin T, Xu L, Chen K (2009) Observation and model of highly ordered wavy cracks due to coupling of in-plane stress and interface debonding in silica thin films. Physical Review B 80(1):014,121

[51] Xia ZC, Hutchinson JW (2000) Crack patterns in thin films. Journal of the Mechanics and Physics of Solids 48(6):1107–1131

[52] Xie ZQ, Sevilla R, Hassan O, Morgan K (2013) The generation of arbitrary order curved meshes for 3D finite element analysis. Comp Mech 51(3):361–374

[53] Xu XP, Needleman A (1995) Numerical simulations of dynamic crack growth along an interface. International Journal of Fracture 74(4):289–324

Preprint of
R. Sevilla and E. Barbieri
NURBS distance fields for extremely curved cracks
Computational Mechanics, 54 (6); 1431-1446, 2014

[54] Yagawa G, Yamada T (1996) Free mesh method: a new meshless finite element method. Computational Mechanics 18(5):383–386

[55] Zhu T, Zhang JD, Atluri S (1998) A local boundary integral equation (lbie) method in computational mechanics, and a meshless discretization approach. Computational Mechanics 21(3):223–235